π-SQUIDs based on Josephson contacts between high-T_c and low-T_c superconductors

H. J. H. Smilde, Ariando, D. H. A. Blank, H. Hilgenkamp,* and H. Rogalla
Faculty of Science and Technology and MESA$^+$ Research Institute, University of Twente, P.O. Box 217, 7500 AE Enschede, The Netherlands
(Received 14 December 2003; published 27 July 2004)

For phase-sensitive studies on the pairing-symmetry in a given superconductor, its combination with a well-characterized isotropic superconductor into a superconducting quantum interference device (SQUID) provides a very fruitful method. With a well-controlled orientation and position of the hybrid Josephson junctions involved, the angular dependence of both the phase and the magnitude of the order parameter wave function can be determined. In view of this, and motivated by recent proposals for quantum-logic devices, we have investigated low-inductance dc SQUIDs with different geometries. These SQUIDs are based on ramp-type $YBa_2Cu_3O_7$/Au/Nb junctions oriented toward the $\langle 100\rangle$-$YBa_2Cu_3O_{7-\delta}$ crystal axes. For SQUIDs with perpendicularly oriented junctions, maxima in the critical current are observed at applied fluxes of $\pm\frac{1}{2}\,\Phi_0$, confirming the predominant $d_{x^2-y^2}$ pairing symmetry in $YBa_2Cu_3O_7$. The measured critical current-modulations for these π-SQUIDs correspond well to simulations. No indications are found for any time-reversal symmetry breaking, for instance resulting from imaginary symmetry admixtures.

DOI: 10.1103/PhysRevB.70.024519 PACS number(s): 74.20.Rp, 85.25.Dq, 74.78.Bz, 85.25.Am

I. INTRODUCTION

Superconducting quantum interference devices (SQUIDs) present excellent tools to perform phase-sensitive experiments on the order parameter symmetry in superconductors.[1–6] In a dc SQUID in which an isotropic *s*-wave superconductor contacts the superconductor to be studied in two crystal orientations, the critical current versus the applied magnetic flux dependence contains information about the relative phase and magnitude at both contacts. This principle is employed here to study the order parameter symmetry of the high-T_c superconductor $YBa_2Cu_3O_7$, using the low-T_c superconductor Nb as the counter electrode. Previous SQUID experiments on the order parameter symmetry of the high-T_c cuprates have been performed using for example Pb as counter electrode. In this, single crystals[3] of $YBa_2Cu_3O_7$ as well as twinned and untwinned thin films[4,5] have been used. These SQUIDs generally had inductances of $LI_c \approx \Phi_0$ or larger. Here, we focus principally on low-inductance SQUIDs. This enables a more precise analysis, as will be pointed out below. Recently, low-inductance all-high-T_c π-SQUIDs have been prepared using tetra-crystal substrates, providing clear evidence for predominant $d_{x^2-y^2}$ wave order parameter symmetry.[6] These dc π-SQUIDs were based on symmetric 45° [001]-tilt grain-boundary junctions. By definition, grain-boundary junctions are subject to limitations with respect to the orientation of the superconductors on both sides of the junction interface. Additionally, a complicating factor is presented by the fact that both electrodes are characterized by the order parameter symmetry under investigation. Junctions combining a well-characterized isotropic superconductor with the superconductor to be studied provide the ability to probe the order parameter in any desired orientation. For this reason, and motivated by recent suggestions for quantum-logic devices based on contacts between *s*-wave and *d*-wave superconductors,[7,8] we have developed ramp-type junctions between $YBa_2Cu_3O_7$ and Nb.[9] These junctions are employed here for the fabrication of low inductance dc SQUIDs.

In the following, first, theoretical considerations of importance for the understanding of π-SQUIDs are introduced. These include aspects of phase-coherence, the formulation of SQUID dynamics with an additional phase-shift, spontaneous flux and *S* states, and the magnetic field dependence of the π-SQUID critical current. Subsequently, the preparation and experimental characterization of the low inductance dc SQUIDs is presented, and the results and implications, particularly with respect to the order parameter symmetry, are discussed.

II. THEORETICAL ASPECTS

The single-valued phase of the charge-carrier condensate in a superconductor results in quantization of the magnetic flux enclosed by a superconducting loop. For a dc SQUID it holds accordingly that the accumulated phase around the SQUID loop including the phase-differences over the two Josephson junctions is limited to multiples of 2π. Depending on the orientation of the junctions, unconventional order parameter symmetry can induce an additional phase-shift ε in the loop. The single-valuedness of the wave function around the SQUID loop then requires:

$$k2\pi = \varphi_2 - \varphi_1 + \varepsilon + (2\pi/\Phi_0)(\Phi_a + L_2 I_2 - L_1 I_1) \qquad (1)$$

where φ_i is the phase-difference over the junctions having critical current I_{ci}, and L_i is the partial inductance on the sides of the SQUID loop indicated with the index i = 1 and 2. The applied magnetic flux is given with Φ_a. In a general approach (RCSJ-model), the total current I_i through junction i consists of the sum of the supercurrent I_{si}, the normal or quasi-particle current, the displacement current and a noise term. Here, we will consider mainly properties related to the supercurrents through the junctions. These are given by the

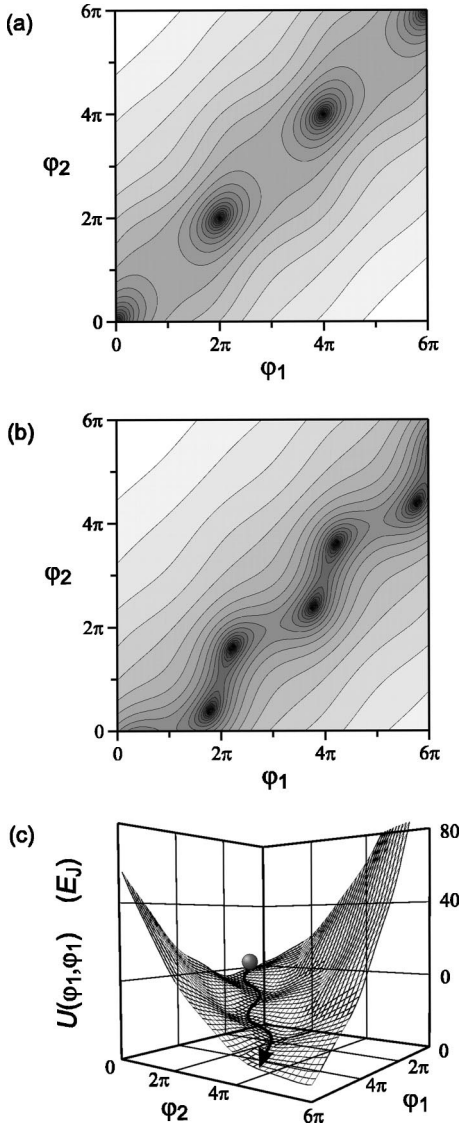

FIG. 1. Potential surface $U(\varphi_1,\varphi_2)$ of a SQUID (a), and of a π-SQUID (b) with identical parameters given by: $L=5.2$ *p*H, $I_c=100$ μA $(=\frac{1}{2}\ I_{c,\mathrm{SQUID}})$, $\alpha_J=0.2$, and $\alpha_L=0$, and in the absence of an externally applied magnetic field or bias current. The energy is plotted on a logarithmic scale with an offset of $+0.01\ E_J$ for the SQUID and $-1.28\ E_J$ for the π-SQUID to stress the minima (black). (c) 3D perspective view of the potential surface of the π-SQUID in (b), here with a bias current of $I_{\mathrm{bias}}=200$ μA. A possible trajectory of the particle with mass M is schematically indicated.

first Josephson relation $I_{si}=I_{ci}\sin(\varphi_i)$, assuming a sinusoidal current-phase relation for both junctions. All flux-related terms in Eq. (1) are normalized to the flux quantum $\Phi_0=2.07\times10^{-15}$ T m^2. If an order parameter symmetry-induced phase shift is present along the loop, ε has a value between 0 and 2π. By convention, the positive current direction is chosen to be toward the ground, and the order parameter-induced phase shifts are considered to be positive when following the clockwise direction going around the SQUID loop.

A. SQUID dynamics

Using the RCSJ model for both junctions, the dynamic behavior of the SQUID can be described with the analogy of a particle with an effective mass M_{ij} moving under influence of gravity described by a potential $U=U(\varphi_1,\varphi_2)$ and in the presence of a damping force G_{ij}:[10]

$$M_{ij}\partial^2\varphi_i/\partial t^2 = -\nabla U - G_{ij}\partial\varphi_i/\partial t \tag{2}$$

where $M_{ij}=C_{ij}\Phi_0^2/(2\pi)^2$ and $G_{ij}=\Phi_0^2/[(2\pi)^2R_{ij}]$. Both are 2×2 matrices, with C_{ii} and R_{ii} the capacitances and resistances of the individual junctions. The off-diagonal elements are 0. Being aware that the bias current is the sum of the total currents through both junctions and with the notations $I_{c1}=(1+\alpha_J)I_c$, $I_{c2}=(1-\alpha_J)I_c$, and $L_1=\frac{1}{2}(1+\alpha_L)L$, $L_2=\frac{1}{2}(1-\alpha_L)L$, it can be shown that using the condition in Eq. (1) the potential surface U is given by

$$\begin{aligned}U(\varphi_1,\varphi_2) = E_J\Big\{&\tfrac{1}{2}K(\varphi_2-\varphi_1+\varepsilon+\phi_a)^2 - i_B[(1-\alpha_L)\varphi_1\\ &+(1+\alpha_L)\varphi_2] + (1+\alpha_J)(1-\cos\varphi_1)\\ &+(1-\alpha_J)(1-\cos\varphi_2)\Big\}.\end{aligned} \tag{3}$$

In this, the degree of asymmetry in the SQUID inductance and the junction critical currents are specified with α_L and α_J, respectively. The energy is expressed in units of the Josephson energy $E_J=hI_c/4\pi e$, and the additional normalizations $K=(\Phi_0/2\pi LI_c)$, $\phi_a=2\pi\Phi_a/\Phi_0$, and $i_B=I_{\mathrm{bias}}/2I_c$ are used in Eq. (3), with I_c the average junction critical current. Figure 1 shows contour plots of two potential-energy surfaces as a function of the phase differences over the junctions, for a standard SQUID (a) and a π-SQUID (b). If a bias current is applied, the surface will be tilted along the $\varphi_2=\varphi_1$ direction, modifying the junction phase differences with an equal rate. For a bias current equal to or larger than the SQUID critical current, the particle with mass M will move along this direction. This is illustrated in Fig. 1(c), presenting a three-dimensional (3D) surface plot of the potential with a possible trajectory of the particle. On the other hand, application of an external flux corresponds to a tilt of the potential surface in the perpendicular $\varphi_2=-\varphi_1$ direction. With this, a growing *difference* in the junction phase differences indicates an increasing amount of flux in the SQUID ring. It is remarked that the behavior of a π-SQUID ($\varepsilon=\pi$) is basically identical to the behavior of a SQUID biased with a constant external background flux of $\frac{1}{2}\Phi_0$.[11–14]

In Fig. 1 the SQUIDs are in the low-inductance regime, $LI_c<\Phi_0$, and have identical parameters. No magnetic flux is applied externally. The standard SQUID presents minima in the energy for $\varphi_2=\varphi_1$ at an integer number of 2π, and no currents flow. On the contrary, the number of minima has doubled for the π-SQUID and their positions deviate from integer numbers of 2π. To accentuate the doubling of the minima a slight asymmetry in junction critical current, $\alpha_J=0.2$, was taken for both SQUIDs. The minima are degenerate in energy for $\varepsilon=\pi$, and correspond to a spontaneous current in clockwise or counterclockwise direction in the π-SQUID ring. It is suggested to profit from these spontaneously circulating currents as a self-bias in, e.g., RSFQ-logic as a means to reduce the number of bias lines.[15,16] Further-

more, the intrinsic degeneracy of the energy minima in the π-phase biased (SQUID-)loop may offer prospects for qubit design; the sensitivity to flux noise may be diminished by a design using reduced dimensions of a π-phase biased loop[16] without loss of the twofold degenerate state. Additionally, noise introduced by a static externally applied magnetic field, which is used for the preparation of the degenerate state in the unbiased loop, is avoided.

B. Spontaneous magnetic flux

The self-generated current circulating in the π-SQUID ring induces a spontaneous magnetic flux. In an early paper, Copetti *et al.*[17] described the spontaneous flux in π-SQUIDs using an instructive approach. A further analysis was provided by Kirtley *et al.* for contacts between standard and π-junctions.[18] To evaluate the spontaneous flux in a π-SQUID ring, the applied magnetic field and the bias current are set to zero, and only supercurrents are considered. The expression of the free-energy, Eq. (3), can then be written in the common form as the sum of the magnetic energy in the ring due to the circulating current and the Josephson energies of both junctions: $U=\frac{1}{2}LI_{\mathrm{cir}}^2+\Sigma_{i=1,2}E_{Ji}(1-\cos(\varphi_i))$. The minimum energy is determined numerically under condition (1). Figure 2 presents the corresponding behavior of the junction phase-differences and the spontaneous magnetic flux versus the normalized inductance times the smallest of the critical currents I_c. The ratio of both junction critical currents is given by γ ($I_{c2}=\gamma I_{c1}=\gamma I_c$, $\gamma \geqslant 1$). A different notation is used here, compared to Sec. II A, for the (asymmetry in) junction critical currents to facilitate the evaluation in the limit of the one-junction SQUID ($\gamma \to \infty$), i.e., the rf SQUID. Generally, fractional flux (Φ_0/f with $f \geqslant 2$) is spontaneously generated for a minimum loop inductance of $LI_c \geqslant (\Phi_0/2\pi)\,[1-(1/\gamma)]$, assuming $\varepsilon=\pi$. For growing inductance the self-generated flux asymptotically converges to $\frac{1}{2}\Phi_0$, and the junction phase differences relax to zero decreasing the junctions' energies. In the limit of a low inductance, the phase-difference of the smallest junction becomes π, while the larger junctions' phase-difference is zero. No circulating current flows. An exception is the completely symmetric π-SQUID, which is able to sustain a phase-difference of $\pi/2$ over both junctions, even in the theoretical zero-inductance limit. Although in this case the maximum supercurrent circulates, the spontaneous flux decreases to zero reducing the ring size, as it is proportional to its inductance.

Let us now analyze the conditions for which the maximum supercurrent flows in the ring. The phase-difference over the smallest junction then equals $\pi/2$. This is expressed as $LI_c=(\Phi_0/2\pi)\,[\pi/2-\arcsin(1/\gamma)]$, which yields, e.g., for the rf-SQUID a spontaneous flux of $\frac{1}{4}\Phi_0$ at the maximum circulating supercurrent. Remark that, on the contrary, the maximum spontaneous flux of $\frac{1}{2}\Phi_0$ is generated in the limit for infinite loop-inductance, while the circulating supercurrent tends to zero.

If the phase-shift induced by the order parameter is not exactly π (or zero), the order parameter presents time-reversal symmetry breaking. In this case, the self-generated

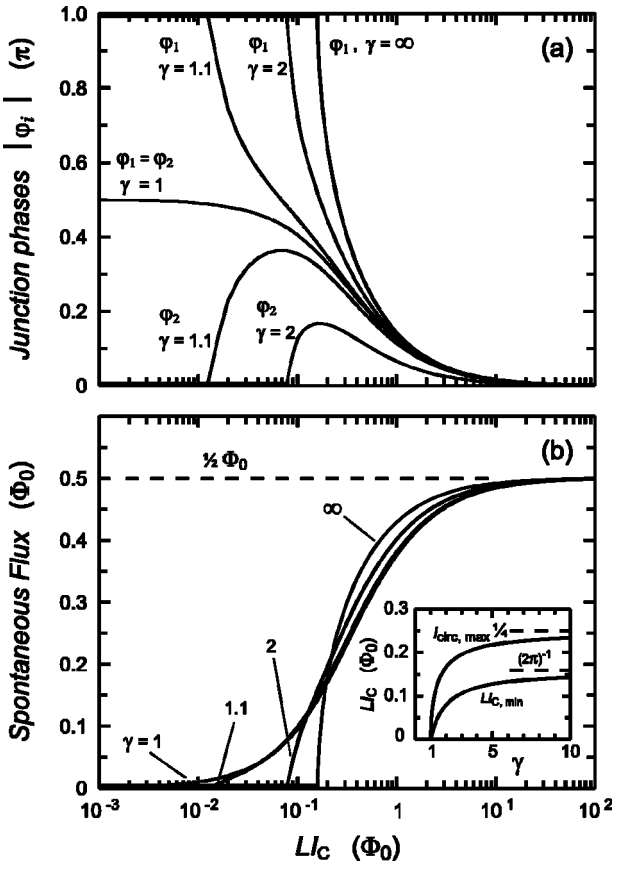

FIG. 2. Spontaneous flux in π-SQUIDs for varying inductance LI_c, and ratio of the junction critical currents γ: (a) Behavior of the junction phase-differences, and (b) the corresponding self-generated magnetic flux. The simulation is normalized to the smallest of the junction critical currents I_{c1}: $I_{c2}=\gamma I_{c1}=\gamma I_c$ with $\gamma \geqslant 1$. For $\gamma \to \infty$ the π-SQUID-ring contains effectively only one junction. In the inset of (b) the minimum inductance LI_c is presented for varying γ above which flux is generated, and the dependence for which the maximum current is circulating in the π-SQUID-ring ($\varphi_1=\pi/2$).

clockwise and counterclockwise currents have different magnitudes, and a difference in the amount of spontaneous flux for both states should be detected.[2] Here, the superconducting states, the *S* states,[19] are analyzed as the relation of the total flux in the loop ϕ_t and the externally applied flux ϕ_a, both expressed in terms of phase. In the following, the SQUID inductance is normalized as $\lambda=(2\pi/\Phi_0)LI_c$, with I_c the (smallest of the) junction critical current(s). The total flux in a rf SQUID is given by $\phi_t=\phi_a+\lambda\sin(\varphi)$, which is the sum of the externally applied flux and the flux due to the circulating current in the SQUID inductance. The single-valuedness of the wave function requires furthermore that $\phi_t=-\varphi-\varepsilon$. This yields the desired relation describing the *S* states and the corresponding energy, with ε the order parameter induced phase-shift:

$$\phi_a = \phi_t + \lambda\sin(\phi_t+\varepsilon),$$

$$U(\phi_a;\phi_t) = E_J\{1-\cos(\phi_t+\varepsilon)+(\phi_a-\phi_t)^2/(2\lambda)\}. \quad (4)$$

Note that ϕ_a is an externally controlled parameter imposing a boundary condition for the total flux in the loop ϕ_t. This similarly holds for the total flux in the dc SQUID $\phi_t = \phi_a + (2\pi/\Phi_0)\{L_2 I_{c,2} \sin(\varphi_2) - L_1 I_{c,1} \sin(\varphi_1)\}$, and $\phi_t = -\varphi_2 + \varphi_1 - \varepsilon$ from phase-coherence in the ring. Additionally, the constraint $I_{c,2} \sin(\varphi_2) + I_{c,1} \sin(\varphi_1) = 0$ holds in the absence of a bias current. For the symmetric dc SQUID ($\gamma = I_{c,2}/I_{c,1} = 1$) one obtains:

$$\phi_a = \phi_t + \lambda \sin\left\{\tfrac{1}{2}(\phi_t + \varepsilon)\right\}\cos(m\pi),$$

with

$$U(\phi_a;\phi_t) = E_J\{2 - 2\cos(m\pi)\cos[(\phi_t + \varepsilon)/2] + (\phi_a - \phi_t)^2/(2\lambda)\}, \quad m = 0,1. \tag{5a}$$

On first sight, Eq. (5a) may seem to imply that the period of the $\phi_t - \phi_a$ dependence is twice the usual Φ_0-periodicity. However, solutions obeying the phase-coherence describe two distinct curves for the symmetric dc SQUID $(\varphi_1, \varphi_2) = (\varphi_i, -\varphi_i)$ and $(\varphi_j, 2\pi - \varphi_j)$, for which the circulating supercurrent drives the flux in the ring toward an even ($m=0$) or an odd number ($m=1$) in Φ_0, respectively (with an offset of $\varepsilon\Phi_0/2\pi$ if $\varepsilon \neq 0$). As a result, the *S* states of the symmetric dc SQUID are periodic with a period of Φ_0 as expected. The slightest asymmetry in the dc SQUID ($\gamma > 1$) eliminates the apparent $2\Phi_0$ periodicity with two solutions of the *S* states, and characteristics comparable to the rf SQUID *S*-states result. Using analogous arguments as for the symmetric dc SQUID, it can be shown that the *S* states of an asymmetric dc SQUID are described by

$$\phi_a = \phi_t + \lambda\gamma \sin\{\arctan[\sin(\phi_t + \varepsilon)/(\gamma + \cos(\phi_t + \varepsilon))]\},$$

with

$$U(\phi_a;\phi_t) = E_J\{\gamma - \gamma\cos(\arctan[\sin(\phi_t + \varepsilon)/(\gamma + \cos(\phi_t + \varepsilon))]) + 1 - \cos(\phi_t + \varepsilon - \arctan[\sin(\phi_t + \varepsilon)/(\gamma + \cos(\phi_t + \varepsilon))]) + (\phi_a - \phi_t)^2/(2\lambda)\}, \quad \gamma > 1. \tag{5b}$$

In the limit to the rf SQUID ($\gamma \to \infty$ Eq. (4) is obtained, as $\lim_{\gamma\to\infty} \gamma \sin\{\arctan[\sin(x)/(\gamma + \cos(x))]\} = \sin(x)$. Figure 3 shows the *S*-state diagrams in the usual representation of the total flux in the loop versus the externally applied flux. On the left-hand side (a, c, and e) the SQUID states are presented, while on the right-hand side (b, d, and f) similar π-SQUID characteristics are shown. From top to bottom, first the rf SQUIDs are displayed, then the symmetric dc SQUIDs, and thereafter the asymmetric dc SQUIDs. Although *S* states with negative slope fulfill the phase-coherence condition, only *S* states with positive slope are stable, a proof of which can be found by considering the minima in the potential energy for a fixed externally applied flux. The *S* states of the rf SQUID become multi-valued for $\lambda > 1$ around $\phi_a = (2k+1)\pi + \varepsilon$ with $k \in \mathbb{Z}$. An example of how the SQUID switches between two states n and $n+1$ varying the externally applied magnetic flux is indicated in each graph with arrows. The SQUID inductances are chosen such that for the π-SQUID cases, apart from the $n = \pm\frac{1}{2}$ states, also the first higher-flux states $n = \pm\frac{3}{2}$ can be observed at zero externally applied flux. Approximate values for the "onset" of higher-flux states are $\lambda \approx 7.8$, 6, and 6.7 for the rf SQUID and the symmetric and asymmetric dc π-SQUID, respectively, where the junction asymmetry of the last equals $\gamma = 1.1$. These π-SQUID inductance values are larger than for the case of standard SQUIDs, given by $\lambda \approx 4.6$, 2, and 3.5, respectively, for observation of the first excited states $n = \pm 1$ in the absence of an externally applied magnetic field. It is emphasized that for the ground states as well as for the higher-flux *S* states, though they are called $n = -\frac{1}{2}, 0, \frac{1}{2}, 1, \ldots$ states, the total flux in the SQUID-ring generally $\Phi_t \neq n\,\Phi_0$ for finite inductance. Only in the special case of $\Phi_a = n\,\Phi_0$ the flux in the SQUID-ring equals $\Phi_t = n\,\Phi_0$, which is deduced easily from the *S*-state diagrams.

A time-reversal symmetry breaking order parameter symmetry shifts the characteristics of the *S* states over $\varepsilon \neq k\pi$ with $k \in \mathbb{Z}$ along the diagonal in the diagram. It is straightforwardly shown that with this the spontaneously generated flux at zero applied flux has different magnitude for clockwise and counterclockwise circulating current, and the degeneracy of the π-SQUID ground state is removed.[2]

C. Magnetic flux dependence of the SQUID critical current on order parameter symmetry

The experimental work in this article focuses on the magnetic flux dependence of the critical current, yielding an accurate method to investigate the order parameter symmetry. The characterization of the maximum SQUID supercurrent in an applied magnetic field is a principally different experiment from the detection of self-generated magnetic flux induced by the order parameter symmetry. In the latter experiment, the energy ground state is studied in the isolated system, in which the free energy is given by the sum of the Josephson energy of the junctions and the contribution associated with the circulating current in the loop. The critical current of the SQUID, on the contrary, is obtained by maximizing the supercurrent $I_s = I_{c1}\sin(\varphi_1) + I_{c2}\sin(\varphi_2)$ for given applied magnetic flux, in which both junction phase-differences obey Eq. (1). A rising—externally applied—bias current delivers the energy to the dc SQUID to reach the critical current under this constraint. Subject to the bias current, the junction supercurrents and hence the junction phase-differences change, individually obeying the first Josephson

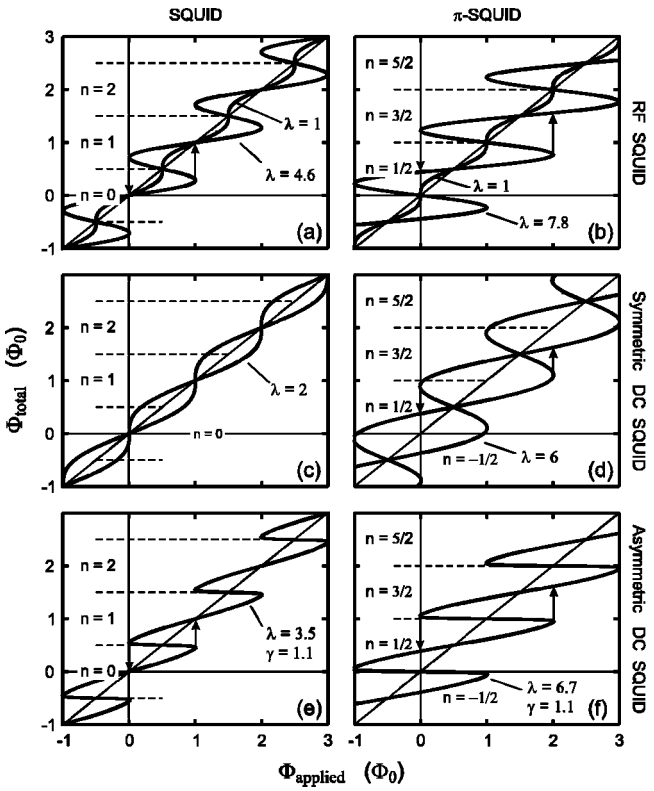

FIG. 3. *S* states in SQUIDs (a, c and e) and π-SQUIDs (b, d and f) for different values of $\lambda=(2\pi/\Phi)\ LI_c$: the total flux in the SQUID-ring as a function of the externally applied flux. In (a) and (b) are the rf SQUIDs presented, in (c) and (d) the symmetric dc SQUIDs, and in (e) and (f) the asymmetric dc SQUIDs with $\gamma=I_{c2}/I_{c1}, \gamma>1$, the degree of asymmetry of the junction critical currents. Curves with negative slope are unstable. The arrows illustrate switching between two *S*-states $n\leftrightarrow n+1$ as the externally applied flux is varied.

relation. Both experiments describe the same system, however in a different situation, and do not exclude each other: a correct measurement of the SQUID critical current is not influenced by possible self-generated flux of the SQUID in the ground state for zero bias current. The critical current versus applied magnetic flux ($I_{c,SQUID}-\Phi_a$) dependence allows for an explicit and straightforward extraction of the order parameter induced phase-shift ε in the SQUID loop. This will be pointed out below with the high-T_c versus low-T_c contacts on which this study concentrates experimentally, in mind.

In the zero-inductance case, $L_1=L_2=0$, the last two terms in Eq. (1) are negligible, and the $I_{c,SQUID}-\Phi_a$ dependence of a SQUID reduces to

$$I_{c,SQUID}(\Phi_a)=\sqrt{(I_{c1}^2+I_{c2}^2+2I_{c1}I_{c2}\cos\{[2\pi\Phi_a/\Phi_0]+\varepsilon\})}. \tag{6}$$

If the high-T_c order parameter is probed by an isotropic superconductor along the same main crystal orientation in a dc SQUID, i.e., both junctions are oriented in parallel, ε equals zero. A maximum critical current is then observed in the absence of an applied magnetic field. In case the junctions are oriented perpendicular with respect to each other in the [100]-directions, the high-T_c order parameter symmetry induces an additional phase-shift in the SQUID-loop. A time-reversal invariant $d_{x^2-y^2}$ order parameter symmetry of the high-T_c cuprate corresponds to a π phase-shift, i.e., $\varepsilon=\pi$, and maxima in the critical current are observed at a magnetic field equivalent to $\pm\frac{1}{2}\Phi_0$. A time-reversal symmetry breaking (TRSB) order parameter, such as predominant $d_{x^2-y^2}$ pairing with an imaginary *s*-wave admixture, results in a deviation from π, and consequently the maximum critical current occurs at an applied flux differing from $\pm\frac{1}{2}\Phi_0$.

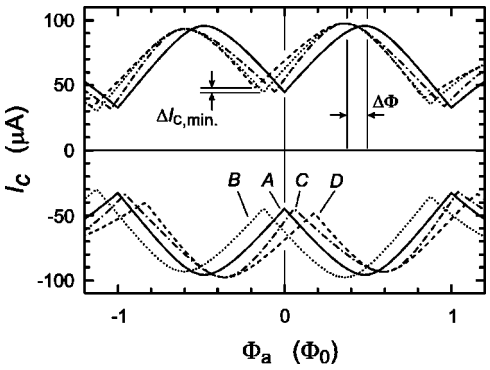

FIG. 4. Simulation of dc π-SQUIDs with finite size junctions. The inductance is $L=16$ *p*H and the $I_{c0,SQUID}=100$ μA. The applied magnetic flux induces three SQUID oscillations within the first zero of the junction Fraunhofer dependence, i.e., $k_i=3$ (A) symmetric π-SQUID, (B) symmetric SQUID with an order parameter induced phase-shift of 0.75 π, (C) asymmetric π-SQUID with $L_1=2\ L_2$, and (D) asymmetric π-SQUID with $I_{c1}=2\ I_{c2}$. The offsets for the latter three all equal $\Delta\Phi=1/8\ \Phi_0$. Only (B) is not point symmetric in the origin. Asymmetry in the junction critical currents (D) yields a reduced modulation depth indicated with the vertical arrows.

For finite inductance, the critical current of a dc SQUID cannot be expressed analytically. Here, the $I_{c,SQUID}-\Phi_a$ dependence for low-inductance dc SQUIDs is calculated numerically using the method of Lagrange multipliers.[20] The order parameter induced phase-shift is taken into account by means of Eq. (1). Besides the SQUID modulation, also the critical currents of the individual junctions are modulated in an applied magnetic field, and a convolution with the SQUID modulation results. Assuming homogeneous rectangular junctions in the small junction limit, the junction modulation is included in the model by taking $I_{ci}(\Phi_a)=I_{c0,i}|\sin(\pi\Phi_a/k_i\Phi_0)/(\pi\Phi_a/k_i\Phi_0)|$, with k_i the ratio of the effective SQUID area over the effective area of junction i with respect to the applied magnetic flux. Numerical simulation shows that the integral junction critical current still complies with a sinusoidal dependence on the phase-difference in the presence of a static applied magnetic flux in the small junction limit, which allows for this procedure.

Figure 4 presents simulations for four (π-) SQUIDs all with $k_i=3$, and all having the same critical current $I_{c0,SQUID}=I_{c0,1}+I_{c0,2}=100$ μA and inductance $L=L_1+L_2=16$ *p*H. As becomes clear below, the influence of asymmetries in the SQUID should be distinguished from order parameter symmetry induced phase-shifts. To discriminate between both effects, the complete $I_{c,SQUID}-\Phi_a$ dependence needs to be reg-

istered, i.e., for positive and negative bias current as well as for positive and negative magnetic flux. The symmetric π-SQUID, curve *A*, presents extremes at $\pm\frac{1}{2}\Phi_0$ and a minimum in the absolute critical current at zero magnetic flux. In case of TRSB order parameter symmetry ($\varepsilon \neq k\pi, k \in \mathbb{Z}$), a deviation in the magnetic flux is observed for curve *B* in the simulation. The deviation is for positive and negative bias-current in the same direction of the applied magnetic flux, and an asymmetric dependence with respect to zero magnetic flux results.

A similar change in the $I_{c,SQUID}-\Phi_a$ dependence is observed for asymmetric π-SQUIDs, curves *C* and *D*, which present a shift in magnetic flux of the *maximum* in the absolute critical current described by

$$\Delta\Phi = L_2 I_{c2} - L_1 I_{c1}. \tag{7}$$

In contrast to the influence of TRSB order parameter symmetry, the shift in magnetic flux changes sign on bias-current reversal in case of different junction critical currents or different partial loop-inductances. Consequently, the $I_{c,SQUID}-\Phi_a$ dependence is point-symmetric in the origin. An additional real *s*-wave admixture to predominant $d_{x^2-y^2}$ order parameter symmetry can give rise to dissimilar junction critical currents. In this case, the superconducting gap is increased along one of the main crystal axis in the $YBa_2Cu_3O_7$ *ab*-plane, while in the orthogonal direction the gap is decreased in magnitude, which leads to a dissimilar Josephson coupling for perpendicular junctions, and a shift in the maxima as described by Eq. (7). Apart from an anti-symmetric $I_{c,SQUID}-\Phi_a$ dependence, dissimilar junction critical currents result furthermore in a reduced modulation depth of the low-inductance SQUID oscillations, which can easily be verified with Eq. (6). The expected modulation depth for a (symmetric) SQUID follows from $100\%/(1+\beta)$, where the screening parameter $\beta = LI_{c,SQUID}/\Phi_0 = 2LI_c/\Phi_0$. Asymmetry in the critical currents yields a reduction in this modulation,[21] the effect of which increases in importance for decreasing loop inductance. It is noted that the *minima* in the absolute critical current are shifted by less than the amount given by Eq. (7), if only an asymmetry in the loop inductance is present and the junction critical currents are identical in magnitude. In that case, the modulation curve becomes deformed. Additionally it is remarked that the maxima of the SQUID critical currents around zero flux are equally raised or lowered for all three origins of identical shift $\Delta\Phi$ in the magnetic flux relative to the symmetric π-SQUID.

The advantage of the use of low-inductance SQUIDs is now straightforwardly clarified. Any SQUID asymmetries present, from fundamental or preparational origin, yield an anti-symmetric shift in the $I_{c,SQUID}-\Phi_a$ dependence smaller than a SQUID oscillation period for $LI_c < \Phi_0$. Using the analysis presented above, SQUID asymmetries can be identified from the $I_{c,SQUID}-\Phi_a$ dependence and related to dissimilar order parameter amplitude and phase in both crystal directions, or to an asymmetric loop-inductance. An order parameter induced phase-shift is recognized unambiguously in the (anti-)symmetric $I_{c,SQUID}-\Phi_a$ dependence as an apparent shift in the applied magnetic flux. Separate test elements placed nearby on the chip, such as SQUIDs with parallel oriented junctions, can be used as an additional verification of zero field. Second, lowering the SQUID inductance increases the weight of the quadratic term in the potential energy (Eq. (3)) due to the applied magnetic flux. In this way, the possibility of higher-flux states is eliminated, and SQUID hysteresis varying the applied magnetic flux is removed as only a single solution is possible for a given range in applied magnetic flux. This facilitates the straightforward registration of the $I_{c,SQUID}-\Phi_a$ dependence. Furthermore, the depth of the SQUID modulation increases for decreasing β, which enhances the measurement accuracy of the extremes in the critical current. Finally, the deviation of the expected modulation depth relating to SQUID asymmetry is more pronounced for decreasing β, and offers in principle, besides the offset $\Delta\Phi$ in Eq. (7), a second parameter to determine the amount of real admixtures.

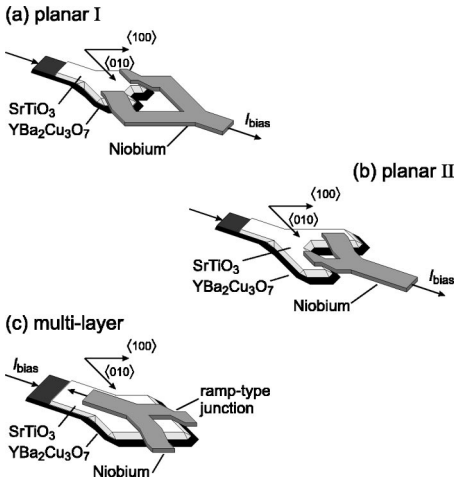

FIG. 5. Design of low inductance π-SQUIDs. (a) Planar design I, (b) planar design II, and (c) multi-layer design.

III. EXPERIMENTAL RESULTS

The geometry and preparation of $YBa_2Cu_3O_7$/Nb SQUIDs are presented first in this section. The SQUIDs with perpendicular oriented junctions, the π-SQUIDs, take a central position in the determination of the order parameter symmetry. The results of the electrical characterization in the presence of a magnetic field are shown, and the electrical properties will be discussed. A detailed discussion on the interpretation of the measurements with respect to the order parameter symmetry is part of the discussion in Sec. IV.

A. Preparation

Various SQUID designs have been realized for this study. They all have a low normalized inductance, $LI_c < \Phi_0$. The different configurations of the π-SQUIDs are indicated schematically in Fig. 5. For comparison, reference SQUIDs incorporating parallel oriented junctions have been fabricated using similar designs. In Fig. 5(a) the first π-SQUID configuration is depicted, in which the isotropic Nb probes two orthogonal directions of the high-T_c superconductor. The SQUID inductance is limited by the minimum linewidth of

the photo-resist stencil applying a standard photolithographic process, yielding usually inductances of $\geqslant 10$ pH for this configuration. Using the second design, Fig. 5(b), the minimum dimensions of the SQUID hole are set by the alignment accuracy of the Nb lift-off mask with respect to the base electrode, and the inductance can be reduced to approximately 4 pH for a $2-3$ μm hole diameter. It is noteworthy that in the second design an electron trajectory around the loop virtually experiences three order parameter induced phase-shifts, for the direction is changed three times over 90° inside the high-T_c superconductor. Apart from the planar SQUID-washers, the ramp-type junction configuration also permits the use of multi-layers for the definition of the SQUID-loop, as shown in Fig. 5(c). The loop dimension is reduced in one direction, and is defined by the thickness of the insulating layer. With a 100 nm $SrTiO_3$ layer and using a standard photolithographic process, loop inductances in the 1 pH range are readily prepared. The availability of these very low loop-inductances could present an advantage for phase-biased quantum logic, such as phase-qubits. The (self-generated) flux, the corresponding phase-shift $\Delta\varphi = 2\pi L I_S/\Phi_0 \propto L$ over the inductor, as well as the coupling to environmental flux-noise are minimized in this design.

The preparation procedure will be discussed briefly. Further details about the junction fabrication are described elsewhere.[9] First, bi-layers of [001]-oriented $YBa_2Cu_3O_7$ and $SrTiO_3$ are prepared using pulsed laser deposition on $SrTiO_3$ single-crystal substrates. The $YBa_2Cu_3O_7$ thin films are twinned on a scale of 100 nm and have a zero-resistance transition temperature of 89 K. Ramps are ion-milled in the bi-layers for the realization of the ramp-type junctions. With the same ion-mill step, the structure definition of the SQUID base-electrodes is realized. The ramps in the $YBa_2Cu_3O_7$ base-electrode are aligned along the $\langle 100\rangle$-crystal axes. Similar characteristics for perpendicular-oriented ramps are obtained by choosing a fixed in-plane mill angle parallel to the $\langle 110\rangle$-direction of the $YBa_2Cu_3O_7$ crystal, or by rotational milling, both using a preset angle with the substrate plane. Subsequently, a high-quality interface to the Au-barrier layer is prepared using the interlayer concept,[9] followed by the Nb top-electrode using a lift-off process. The obtained interface transparencies relate to normal state resistance (R_nA) values of $\sim 10^{-12}\ \Omega\,m^2$ at liquid helium temperature. By adapting the Au-barrier thickness d_{Au}, the junction critical current density can be tuned in a wide range from $10^5\ A/m^2$ for $d_{Au} \sim 120$ nm, up to values approaching $10^9\ A/m^2$ for $d_{Au} \sim 7$ nm. In this way, the critical current of a 10-μm-wide junction with a 150-nm-thick base electrode can be set from below 1 μA up to 1 mA at liquid helium temperatures. In addition to the SQUID layout, the Au-barrier thickness is thus another parameter that can be employed to obtain a suitable value of LI_c/Φ_0.

B. Characteristics

The planar SQUID structures are characterized for the behavior of the critical current in an applied magnetic field. The sample area is shielded with μ-metal and with Nb-shielding; rest-fields are estimated to be below 0.3 μT. The applied magnetic field is directed perpendicular to the substrate plane. Even with the unconventional overlap geometry of the ramp-type Josephson junction, Fraunhofer-like I_c-B dependencies are obtained for the individual $YBa_2Cu_3O_7$/Nb ramp-type junctions using this magnetic field orientation.[9] All $YBa_2Cu_3O_7$/Nb Josephson junctions prepared in this study have critical current densities of below $3.4\times 10^7\ A/m^2$. With this, the Josephson penetration depth is estimated to be $\geqslant 5$ μm for the junctions, and all junctions having a width up to 10 μm are considered to be in the small junction limit. Figure 6 shows an I_c-B dependence of a SQUID with parallel aligned junctions (bottom). The black areas in Fig. 6 represent the SQUID modulation in the applied magnetic field. A convolution with the junction modulation is immediately identified. The I_c-B dependence of a π-SQUID having a comparable geometry, however with orthogonal oriented junctions [Fig. 5(a)], is presented in the top part of Fig. 6. The insets show an enlargement around zero field, in which the SQUID modulation is clearly observed. The small black areas in the inset, shown at the highest I_c values of the curves, are due to the hysteresis in the I-V characteristics of the junctions. The $I_{c,SQUID}$-B dependencies are close to completely symmetric. Given the slight anti-

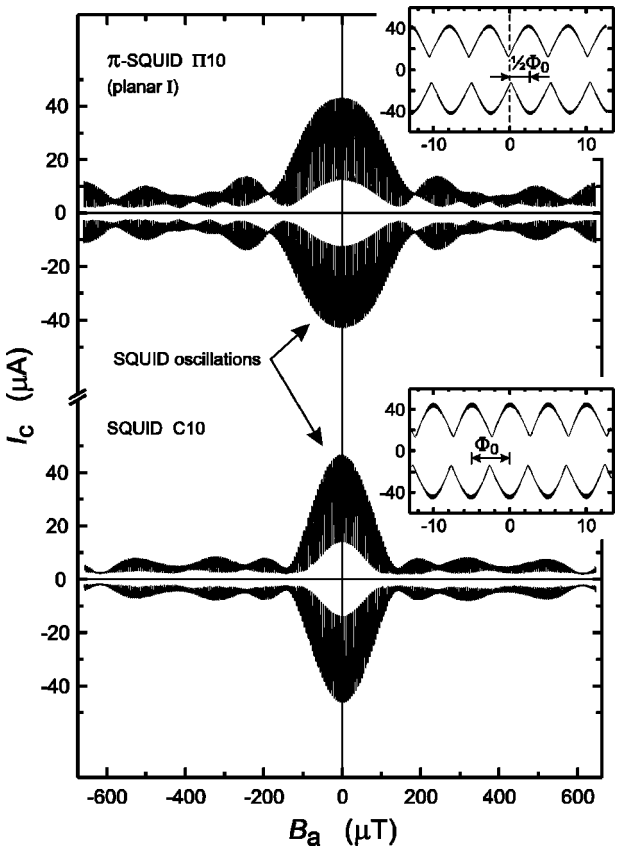

FIG. 6. Critical current as a function of the applied magnetic field at $T=4.2$ K of π-SQUID Π10 with the planar I design (top), and "standard" SQUID C10 (bottom). The insets present an enlargement of the $I_{c,SQUID}$-B dependence near zero field. Both SQUIDs are in the low inductance limit. The magnetic field is applied perpendicular to the substrate plane and the characteristics are recorded with a voltage criterion of 2.5 μV.

symmetry due to dissimilar junction critical currents as described by Eq. (7), the maxima in the critical current at $\pm\frac{1}{2}\Phi_0$ confirm predominant $d_{x^2-y^2}$ order parameter symmetry in $YBa_2Cu_3O_7$. The accuracy in the determination of the magnetic flux is 0.01 Φ_0. The envelope-function given by the junction modulation in the $I_{c,SQUID}$-B dependencies deviates from the ideal Fraunhofer diffraction pattern for higher order oscillations, which is clearly visible in Fig. 6. Minor differences in the effective areas of both junctions, which cause different periods of oscillation in a magnetic field, may induce such behavior. The overlaps of the Nb top electrode over the junction area can be different due to, e.g., the alignment accuracy of the Nb lift-off stencil with respect to the base electrode, and as a result the shielding by the overlaps will be different. Furthermore, the I_c-B dependence of the individual junctions may vary due to a slightly varying current density along the junctions, which influences the magnetic field behavior of the two-junction interferometer. In Fig. 7 (top) the magnetic field dependence of a π-SQUID with the second design of Fig. 5 and a similar standard SQUID (Fig. 7 middle) are depicted. The perpendicular-junction SQUID presents also for this design maximum critical currents at $\pm(\frac{1}{2}\pm 0.01)\Phi_0$, evidencing an order parameter induced phase-shift of $\varepsilon=(1\pm 0.02)\pi$ for orthogonal directions along the main crystal axes in the *ab* plane. In this configuration, the ratio of the SQUID effective area over that of the junctions is decreased as compared to the situation of Fig. 6, and a reduced number of SQUID oscillations are observed within the junction envelope-function. A simulation of dc π-SQUID Π3 is presented in Fig. 7 (bottom) with the corresponding parameters and using an order parameter induced phase-shift of π. The junction-induced envelope over the SQUID oscillations is clearly visible. The different effective area ratios that are used ($k_1=3.7$ and $k_2=4.7$) result in irregular interference, for instance at an applied magnetic flux around $\pm 4\ \Phi_0$. The overlap for the junctions of this π-SQUID, 4 μm and 5.7 μm, respectively, indicates that such a large difference in effective area may well be a realistic estimate. The anti-symmetry in the $I_{c,SQUID}$-Φ_a dependence relating to a difference in junction critical currents corresponds to $\Delta\Phi=0.015\ \Phi_0$.

The effective area of the SQUIDs can be deduced from the period of the SQUID oscillations. One SQUID oscillation corresponds to the in- or outflow of one flux-quantum Φ_0 in the SQUID-loop. Divided by the magnetic flux density ΔB to accomplish this, it yields the effective area of the SQUID-washer: $A_{eff}=\Phi_0/\Delta B$. In general, the effective area of a square washer is estimated with $A_{eff}=c\ d\ D$ if $3d<D$,[22] where c is a constant of the order of unity and d and D are the linear SQUID-hole and SQUID-washer dimension, respectively. A slightly modified expression is used here to estimate the effective area for SQUIDs having minor deviations from a square geometry: $A_{eff}=c\sqrt{(A_{hole}A_{washer})}$, using the hole and the rectangular washer area as input. Comparison with the effective area deduced from the SQUID oscillations yields $c\sim 1.4$–2.0, depending on the exact geometry, which is a realistic value.

The effective area of a junction is usually described with $A_{eff,JJ}=w_{JJ}t$, the junction width multiplied by the effec-

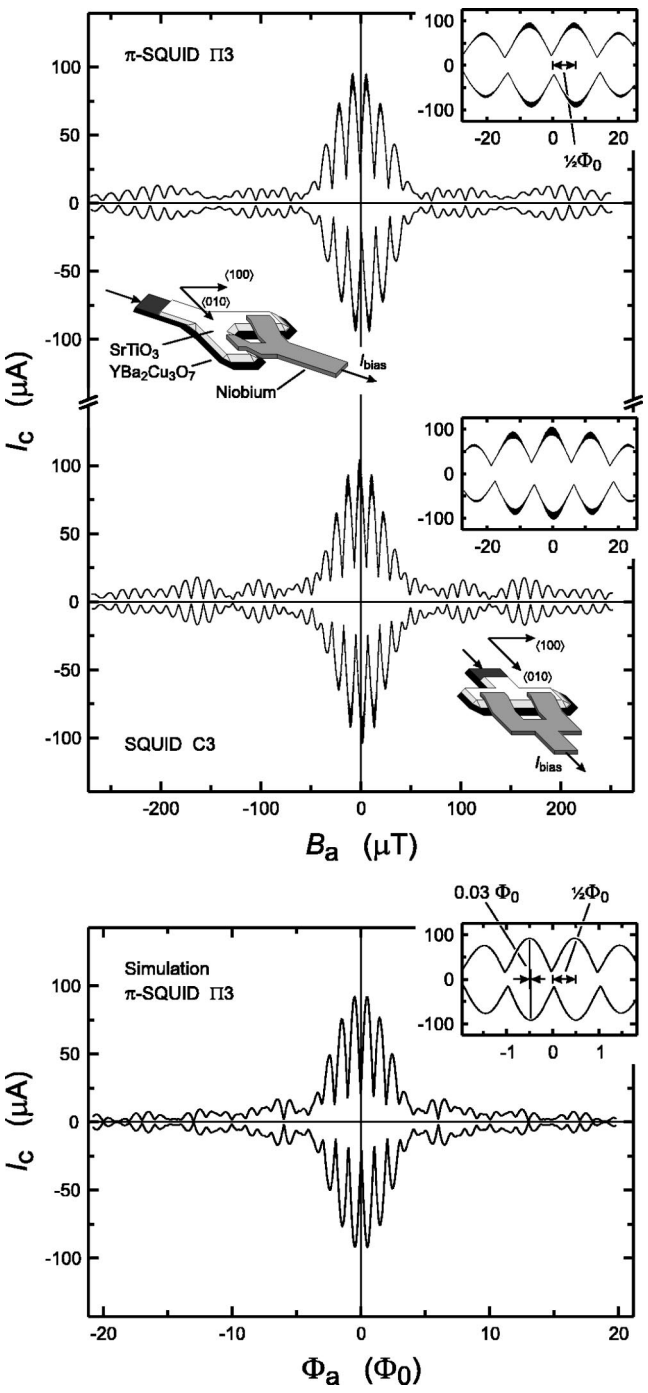

FIG. 7. Critical current as a function of the applied magnetic field at $T=4.2$ K of π-SQUID Π3 with the planar II design (top), and "standard" SQUID C3 (middle). The insets present schematically the corresponding configuration and an enlargement of the $I_{c,SQUID}$-B dependence near zero field. Both SQUIDs are in the low inductance limit. The magnetic field is applied perpendicular to the substrate plane and the characteristics are recorded with a voltage criterion of 2.5 μV. Simulation (bottom) with method of Langrangian multipliers of the $I_{c,SQUID}-\Phi_a$ dependence of dc π-SQUID Π3 using an order parameter induced phase-shift of π. The employed parameters are $L_1=2.4\ p$H, $L_2=2.0\ p$H, $I_{c1}=50.8\ \mu$A, $I_{c2}=43.2\ \mu$A, and $k_1=3.7$, $k_2=4.7$. The shift of the peak positions from $\frac{1}{2}\ \Phi_0$ is $\Delta\Phi=0.015\ \Phi_0$, resulting in a difference in peak position for positive and negative bias-current of 0.03 Φ_0.

TABLE I. A selection of the various SQUIDs that have been prepared and characterized. The critical currents have been designed to be easily measurable, while keeping the individual junctions in the small junction limit meeting $J_c \leqslant 3.4\times10^7$ A/m^2. ($\lambda_J \geqslant 5$ μm). For the different SQUID configurations see Fig. 5.

	Config.	$\Phi_0/\Delta B$ (μm^2)	w_{JJ} (μm)	k_i	$I_{c,SQUID}$ (μA)	L_{geo} (pH)	LI_c/Φ_0	$\lvert L_2Ic_2-L_1Ic_1\rvert$ (Φ_0)
C10	Planar	411	10	31	46.7	15.7	0.35	0.011
Π10	Planar I	397	10	35	43.5	15.7	0.33	0.020
C1	Planar	78	6	4.5	50.5	4.7	0.12	0.013
Π1	Planar II	72	4	6	31.1	3.9	0.06	0.018
C2	Planar	138	4	13	36.5	7.9	0.14	0.000
Π2	Planar II	141	4	12	32.9	7.9	0.13	0.014
C3	Planar	169	10	4.5	103.2	4.7	0.23	0.020
Π3	Planar II	146	10	4.3	94.0	4.4	0.20	0.015
C4	Planar	274	10	6.5	57.5	7.9	0.22	0.091
Π4	Planar II	258	10	6	50.5	7.9	0.19	0.125
Cm	Multi	$\sim$8	10	$\sim$1	349.5	0.9	0.15	-
Πm	Multi	$\sim$2	4	$\sim$1	87.3	0.6	0.03	0.013

tive dimension of the barrier perpendicular to the magnetic field. The latter is estimated as the sum of the barrier thickness and the London penetration depths on both sides of the junction. Correcting for the finite thickness of the electrodes, this is described by $t=\{d_{Au}+\lambda_{Nb}\coth(d_{Nb}/\lambda_{Nb})+\lambda_{YBCO}\coth(d_{YBCO}/\lambda_{YBCO})\}$ with d_{Au} the barrier thickness, and λ_{YBCO} and λ_{Nb} the London penetration depths of the electrode materials with thickness d_{YBCO} and d_{Nb}, respectively. A typical Au barrier thickness of 50 nm and electrodes with a thickness of 150 nm yields $t\sim0.3$ μm. However, the finite film thickness causes the (shielding) currents to spread over a wider lateral area, an effect commonly referred to as flux focusing.[23–26] The area through which the magnetic field threads close to the junction appears therefore enhanced, being on the order of w_{JJ}^2 rather than $w_{JJ}t$. The convolution of the SQUID and junction modulation provides an alternative measure for the effective junction area. The effective junction area for the applied magnetic field is estimated by dividing of the SQUID effective area by the ratio k_i. In this, k_i is determined from the number of SQUID oscillations within the first junction oscillation in the I_c-B dependence. Typical values for the effective junction area derived in this way, are indeed a factor of 10 to 20 larger than obtained from $A_{eff,JJ}=w_{JJ}t$, which confirms the flux focusing effect. Table I summarizes properties of a selection of the characterized SQUIDs, including approximate values for the ratio k_i.

In the I-V characteristics of the planar SQUIDs, LC-resonance structures[27] are observed around the gap voltage depending on the combination of the loop inductance value L and the (average) junction capacitance C. These resonance structures appear at a voltage of $V_r=\{\Phi_0/[2\pi\sqrt{(LC/2)}]\}$ as a result of out-of-phase ac-Josephson oscillations of both junctions. A bias-flux of $\frac{1}{2}\Phi_0$ or an order parameter induced π phase-bias at zero applied flux yields the out-of-phase condition,[28,29] and leads to the LC-resonance structures shown in Fig. 8. For SQUIDs C10 and Π10 the center of the resonance structure is positioned around $V_r\sim75$ μV which corresponds to a junction capacitance of $C\sim2.5$ pF. SQUIDs C3 and Π3 are similarly characterized with $V_r\sim115$ μV, $V_r\sim90$ μV and $C\sim3.5$ pF, $C\sim6$ pF, respectively. The junction capacitance can be determined independently from the hysteresis in the I-V characteristic described by $\beta_C=[2-\alpha(\pi-2)]/\alpha^2$ following Zappe[30] with α the ratio of the return current over the critical current, and using the Stewart-McCumber parameter defined by $\beta_C=(2\pi/\Phi_0)I_cR_n^2C$. In this, I_c, R_n and C are the junction critical current, normal state resistance and capacitance, respectively. In this way a junction capacitance of 1.7 pF is deduced for SQUIDs C10 and Π10, and 1.1 pF and 0.9 pF for SQUIDs

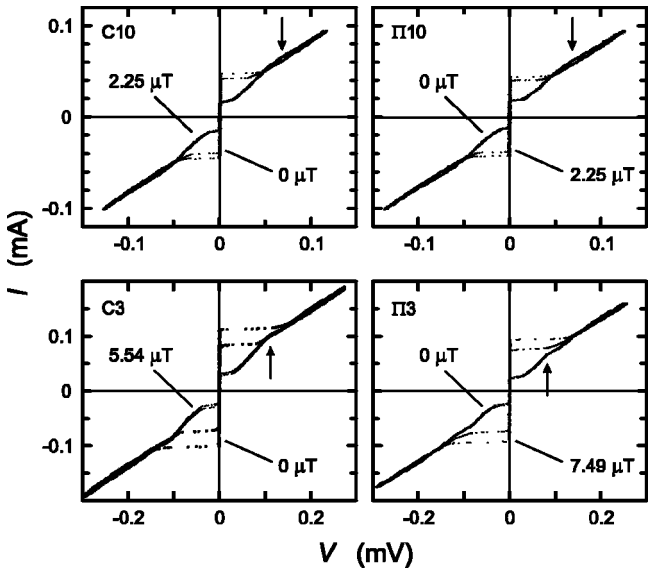

FIG. 8. I-V characteristics at $T=4.2$ K of the SQUIDs and π-SQUIDs corresponding to Figs. 7 and 8: C10, C3, and Π10 and Π3. The SQUIDs are characterized at zero field and at $\frac{1}{2}$ Φ_0. Flux induced or d-wave induced LC-resonance structures are observed for these SQUIDs, indicated with arrows.

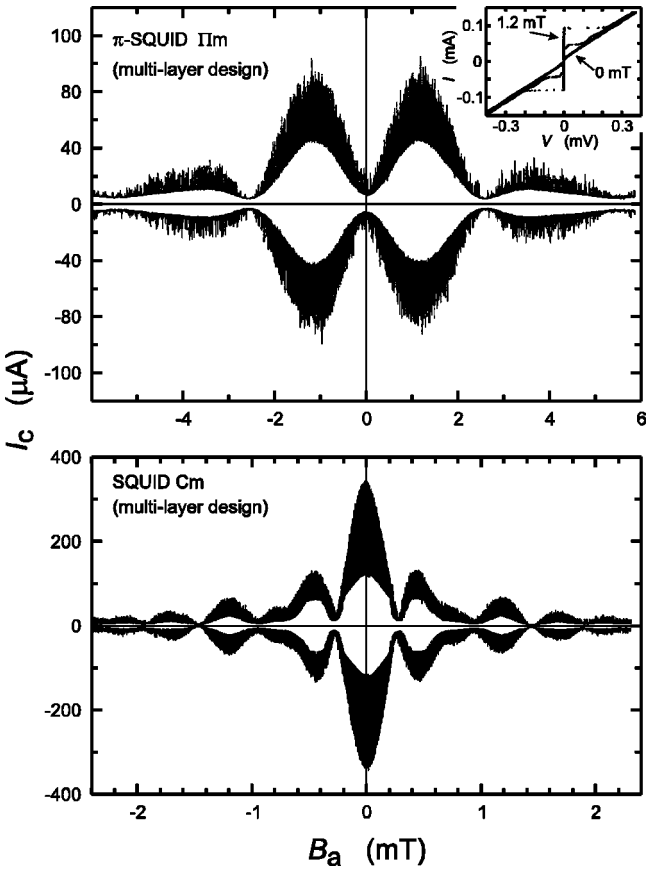

FIG. 9. Critical current as a function of the applied magnetic field at $T=4.2$ K of π-SQUID II*m* (top) and SQUID Cm (bottom), both prepared with the multi-layer design. The SQUIDs are in the low inductance limit. The magnetic field is applied *parallel* to the substrate plane and the characteristics are recorded with a voltage criterion of 5 μV. The *I-V* characteristics in the inset are measured at zero field and for the maximum critical current at $\sim\frac{1}{2}\,\Phi_0$. Resonance structures are observed below the gap voltage at 1.2 mT, probably due to Fiske resonances in the individual junctions.

C3 and II3, respectively. These values are smaller than determined from the position of the resonance peak. A possible explanation is found in the measurement of a smaller critical current of the hysteretic junctions due to preliminary switching to the voltage state, although the *I-V* characteristics have been recorded at a relatively high sweep frequency of 10 Hz.

The multi-layer SQUIDs are characterized with the magnetic field applied parallel to the substrate surface. The effective areas of both the junctions and the SQUID are reduced for this orientation, and larger magnetic fields have to be applied to observe the modulation of the critical current. Figure 9 shows the I_c-B characteristics of the π-SQUID with 4-μm-wide perpendicular junctions (top) and the SQUID with 10-μm-wide parallel junctions (bottom). The black areas reflect the hysteresis in the *I-V* characteristics, which is attributed to an enhanced capacitance of the larger overlap. The noisy signal is ascribed to resonances in the *I-V* characteristics, which hamper the voltage-bias method used to record the I_c-B dependence. For this multi-layer low SQUID-inductance configuration, the ratio of the effective area of the junctions and the SQUID is close to unity, with the used magnetic field orientation. As a result the modulations resemble (corner-)junction behavior. The observation of slightly anti-symmetric maxima at non-zero magnetic field for the SQUID with perpendicular oriented junctions, proves the proper operation of the π-SQUID, and is indicative for predominant *d*-wave symmetry without imaginary admixtures.

IV. DISCUSSION

In the previous sections, it has been pointed out that dc SQUIDs combining an isotropic superconductor with an anisotropic superconductor present an excellent tool for investigations of the order parameter symmetry. Provided that the junctions have identical quality, angle-resolved information about the phase and magnitude of the order parameter can be extracted. The phase is probed by the isotropic superconductor for two crystal orientations of the unconventional superconductor and compared via condition Eq. (1). Anti- or point-symmetric deviations in the I_c-B dependence relate to asymmetries in the loop inductance and the junction critical currents; the latter of which can be recognized as a dissimilar Josephson coupling for both crystal orientations. Excluding a difference in loop inductance by a geometrically symmetric SQUID design, this yields a measure for the relative amplitude of the order parameter comparing both directions. Shifts from zero magnetic field of the center of (anti-)symmetry correlate to the phase of the order parameter. In the following, the investigation of the order parameter symmetry based on the experiments described above and the influence of twinning of the high-T_c superconductor will be considered in more detail.

In the ongoing debate about the exact order parameter symmetry of high-T_c superconductors, subdominant admixtures to the now almost generally established predominant $d_{x^2-y^2}$ order parameter symmetry are under discussion. Especially for $YBa_2Cu_3O_7$, of which the crystal structure is characterized by an orthorhombicity of $(|a-b|/|a+b|)\cong 1\%$ for the optimally doped material, subdominant admixtures can be expected to be present. Generally one distinguishes real and imaginary admixtures, indicating whether the subdominant component acts in-phase or not with the dominant one. Considering the main crystal directions, a real *s*-wave admixture adds to the amplitude of the $d_{x^2-y^2}$-wave symmetry, while an imaginary *s*-wave admixture in addition changes the observed phase (difference) of the order parameter. The amount of imaginary *s*-wave admixture can be estimated using this phase-difference: $|is|/|d|=\tan\{\frac{1}{2}[\pi-(\varphi_{\langle 100\rangle}-\varphi_{\langle 010\rangle})]\}$. Apart from *s*-wave admixtures, also a more complex doping-dependent imaginary id_{xy}-wave admixture has been suggested recently, based on tunneling spectroscopy measurements.[31] The SQUIDs with parallel or orthogonal oriented junctions studied here are insensitive to an imaginary id_{xy}-wave admixture, since only the phase behavior in the main crystal orientations in the *ab* plane is probed. Additionally, only optimally doped $YBa_2Cu_3O_7$ thin films are studied here.

As stated before, all SQUIDs with perpendicular junctions oriented along the $\langle 100\rangle$-crystal axes clearly show I_c maxima

for $\Phi_a = \pm\frac{1}{2}\Phi_0$, which confirms predominant $d_{x^2-y^2}$ order parameter symmetry. A real *s*-wave admixture should induce a dissimilar Josephson coupling for the perpendicular oriented junctions assuming single crystalline $YBa_2Cu_3O_7$, and a difference in junction critical current would result. An antisymmetric $I_{c,SQUID}$-B dependence should be observed in that case. However, our pulsed laser deposited $YBa_2Cu_3O_7$ thin films are twinned on a scale of 100 nm, and the amplitude of the order parameter is rotated over ~90°, since it is coupled to the crystal.[32] Consequently, twinning leads to a total junction supercurrent that results from an ensemble of both crystal-orientations facing the junction. Therefore, a real *s*-wave admixture inducing asymmetric Josephson coupling in the *a*- and *b*-crystal direction is not discernable for our twinned films. Single crystalline films and statistical studies to distinguish from possible slight differences in interface quality for orthogonal directions are needed to determine quantitatively the amount of real *s*-wave admixture.

No evidence for imaginary admixtures has been found in this study within the measurement accuracy. All prepared π-SQUIDs based on the mentioned three designs present I_c maxima at $\pm\frac{1}{2}\Phi_0$ with a precision of below 1% in Φ_0

Thus far, it has been implicitly assumed that on the microscopic level only normal incident charge carriers in the *ab* plane contribute to the supercurrent through the junctions. Sigrist and Rice[33] similarly assumed this when expressing the Josephson current in an all *d*-wave junction. In other words, the tunneling cone[34–36] describing the angular contributions to the Josephson current with respect to the interface normal is taken to be very narrow. This assumption can be understood for the $YBa_2Cu_3O_7/Au/Nb$ junctions in view of the low transparency of $D \sim 10^{-3} \ldots 10^{-4}$ of the $YBa_2Cu_3O_7/Au$ interface.[9] The exponential dependence of the supercurrent density on the Au thickness parallel to the *ab* plane furthermore suggests that, in spite of the beveled ramp-edge, the supercurrent is parallel to the *ab* plane rather than perpendicular to the ramp interface.[9] It is remarked that an averaging effect is expected of the order parameter amplitude in the *ab* plane for a wider tunneling cone or when the interface is faceted, hampering a straightforward determination of a real *s*-wave component from the measurement.

V. CONCLUSION

In summary, aspects of using SQUIDs between an isotropic superconductor and an anisotropic superconductor for the detection of the unconventional order parameter symmetry, and aspects characteristic for SQUIDs incorporating an additional phase-shift, have been considered theoretically. The experimental I_c-B dependencies of the $YBa_2Cu_3O_7/Nb$ SQUIDs with different designs and junction orientations all support predominant $d_{x^2-y^2}$ wave order parameter symmetry. Twinning of the thin film prevents the determination of possible real admixtures, which could arise based on the orthorhombicity of the $YBa_2Cu_3O_7$ crystal. No evidence has been found for imaginary admixtures. The presented experimental characteristics demonstrate the high quality of the SQUIDs that can be obtained from combining an oxide and a metallic superconductor, which facilitates the realization of novel phase-biased superconducting circuits employing the anisotropy of the order parameter.

ACKNOWLEDGMENTS

The authors acknowledge valuable discussions with A. Brinkman, G. J. Gerritsma, A. A. Golubov, S. Harkema, J. R. Kirtley, J. Mannhart, R. G. Mints, J. P. Plantenberg, G. Rijnders, C. W. Schneider, and C. C. Tsuei. This work is supported by the Dutch Foundation for Research on Matter (FOM), the Netherlands Organization for Scientific Research (NWO), and by the ESF PiShift programme.

*Corresponding author. FAX: ++ 31 53 489 1099. Email address: h.hilgenkamp@utwente.nl

[1] D. J. van Harlingen, Rev. Mod. Phys. **67**, 515 (1995).
[2] C. C. Tsuei and J. K. Kirtley, Rev. Mod. Phys. **72**, 969 (2001).
[3] D. A. Brawner and H. R. Ott, Phys. Rev. B **50**, 6530 (1994).
[4] D. A. Wollman, D. J. van Harlingen, W. C. Lee, D. M. Ginsberg, and A. J. Leggett, Phys. Rev. Lett. **71**, 2134 (1993).
[5] A. Mathai, Y. Gim, R. C. Black, A. Amar, and F. C. Wellstood, Phys. Rev. Lett. **74**, 4523 (1995).
[6] R. R. Schultz, B. Chesca, B. Goetz, C. W. Schneider, A. Schmehl, H. G. Bielefeldt, H. Hilgenkamp, J. Mannhart, and C. C. Tsuei, Appl. Phys. Lett. **76**, 912 (2000).
[7] L. B. Ioffe, V. B. Geshkeinbein, M. V. Feigel'man, A. L. Fauchère, and G. Blatter, Nature (London) **398**, 679 (1999).
[8] G. Blatter, V. B. Geshkenbein, and L. B. Ioffe, Phys. Rev. B **63**, 174511 (2001).
[9] H. J. H. Smilde, H. Hilgenkamp, G. Rijnders, H. Rogalla, and D. H. A. Blank, Appl. Phys. Lett. **80**, 4579 (2002).
[10] C. D. Tesche, J. Low Temp. Phys. **44**, 119 (1981).
[11] E. Ben-Jacob, D. J. Bergman, Y. Imry, B. J. Matkowsky, and Z. Schuss, J. Appl. Phys. **54**, 6533 (1983).
[12] M. Klein and A. Mukherjee, Appl. Phys. Lett. **40**, 744 (1982).
[13] A. Barone and G. Paternò, *Physics and Applications of the Josephson Effect* (Wiley, New York, 1982).
[14] G. Testa, E. Sarnelli, S. Pagano, C. R. Calidonna, and M. Mango Furnari, J. Appl. Phys. **89**, 5145 (2001).
[15] J. P. Plantenberg, M.Sc. thesis, University of Twente, The Netherlands, June 2002.
[16] A. V. Ustinov and V. K. Kaplunenko, J. Appl. Phys. **94**, 5405 (2003).
[17] C. A. Copetti, F. Rüders, B. Oelze, Ch. Buchal, B. Kabius, and J. W. Seo, Physica C **253**, 63 (1995).
[18] J. R. Kirtley, K. A. Moler, and D. J. Scalapino, Phys. Rev. B **56**, 886 (1997).
[19] K. K. Likharev, *Dynamics of Josephson Junctions and Circuits*, 3rd ed. (Gordon and Breach, Amsterdam, 1996), p. 198.
[20] W.-T. Tsang and T. Van Duzer, J. Appl. Phys. **46**, 4573 (1975).
[21] C. D. Tesche and J. Clarke, J. Low Temp. Phys. **29**, 301 (1977).

[22] M. B. Ketchen, W. J. Gallagher, A. W. Kleinsasser, S. Murphy, and J. R. Clem, in *SQUID '85-Superconducting Quantum Interference Devices and their Applications*, edited by H. D. Hahlbohm and H. Lübbig (de Gruyter, Berlin, 1985), p. 865.
[23] P. A. Rosenthal, M. R. Beasley, K. Char, M. S. Colclough, and G. Zaharchuk, Appl. Phys. Lett. **59**, 3482 (1991); **60**, 1519(E) (1992).
[24] R. G. Humphreys and J. A. Edwards, Physica C **210**, 42 (1993).
[25] V. G. Kogan, V. V. Dobrovitski, J. R. Clem, Y. Mawatari, and R. G. Mints, Phys. Rev. B **63**, 144501 (2001).
[26] E. H. Brandt and G. P. Mikitik, Phys. Rev. Lett. **85**, 4164 (2000).
[27] D. B. Tuckerman and J. H. Magerlein, Appl. Phys. Lett. **37**, 241 (1980).
[28] E. A. Early, A. F. Clark, and C. J. Lobb, Physica C **245**, 308 (1995).
[29] B. Chesca, R. R. Schulz, B. Goetz, C. W. Schneider, H. Hilgenkamp, and J. Mannhart, Phys. Rev. Lett. **88**, 177003 (2002).
[30] H. H. Zappe, J. Appl. Phys. **44**, 1371 (1973).
[31] Y. Dagan and G. Deutscher, Phys. Rev. Lett. **87**, 177004 (2001).
[32] K. A. Kouznetsov, A. G. Sun, B. Chen, A. S. Katz, S. R. Bahcall, J. Clarke, R. C. Dynes, D. A. Gajewski, S. H. Han, M. B. Maple, J. Giapintzakis, J.-T. Kim, and D. M. Ginsberg, Phys. Rev. Lett. **79**, 3050 (1997).
[33] M. Sigrist and T. M. Rice, Rev. Mod. Phys. **67**, 503 (1995).
[34] E. L. Wolf, *Principles of Electron Tunneling Spectroscopy* (Oxford University Press, Oxford, 1985).
[35] T. Löfwander, V. S. Shumeiko, and G. Wendin, Supercond. Sci. Technol. **14**, R53 (2001).
[36] C. Bruder, Phys. Rev. B **41**, 4017 (1990).